Author Manuscript

Author Manuscript

Author Manuscript

Author Manuscript

HHS Public Access

Author manuscript

Biochem Biophys Res Commun. Author manuscript; available in PMC 2016 July 17.

Published in final edited form as:

Biochem Biophys Res Commun. 2015 July 17; 463(0): 37–41. doi:10.1016/j.bbrc.2015.05.012.

Sarcolipin and phospholamban inhibit the calcium pump by populating a similar metal ion-free intermediate state

L. Michel Espinoza-Fonseca[*], **Joseph M. Autry**, and **David D. Thomas**

Department of Biochemistry, Molecular Biology, and Biophysics, University of Minnesota, Minneapolis, MN 55455

Abstract

We have performed microsecond molecular dynamics (MD) simulations and protein pK_a calculations of the muscle calcium pump (sarcoplasmic reticulum Ca^{2+}-ATPase, SERCA) in complex with sarcolipin (SLN) to determine the mechanism by which SLN inhibits SERCA. SLN and its close analogue phospholamban (PLN) are membrane proteins that regulate SERCA by inhibiting Ca^{2+} transport in skeletal and cardiac muscle. Although SLN and PLB binding to SERCA have different functional outcomes on the coupling efficiency of SERCA, both proteins decrease the apparent Ca^{2+} affinity of the pump, suggesting that SLN and PLB inhibit SERCA by using a similar mechanism. Recently, MD simulations showed that PLB inhibits SERCA by populating a metal ion-free, partially-protonated E1 state of the pump, E1•H^+_{771}. X-ray crystallography studies at 40-80 mM Mg^{2+} have proposed that SLN inhibits SERCA by populating E1•Mg^{2+}, an intermediate with Mg^{2+} bound near transport site I. To test the mode of SLN inhibition, we performed a 0.5-μs MD simulation of E1•Mg^{2+}-SLN in a solution containing 100 mM K^+ and 3 mM Mg^{2+}, with calculation of domain dynamics in the cytosolic headpiece and side-chain ionization and occupancy in the transport sites. We found that SLN increases the distance between residues E771 and D800, thereby rendering E1•Mg^{2+} incapable of producing a competent Ca^{2+} transport site I. Following removal of Mg^{2+}, a 2-μs MD simulation of Mg^{2+}-free SERCA-SLN showed that Mg^{2+} does not re-bind to the transport sites, indicating that SERCA-SLN does not populate E1•Mg^{2+} at physiological conditions. Instead, protein pK_a calculations indicate that SLN stabilizes a metal ion-free SERCA state (E1•H^+_{771}) protonated at residue E771, but ionized at E309 and D800. We conclude that both SLN and PLB inhibit SERCA by populating a similar metal ion-free intermediate state. We propose that (i) this partially-protonated intermediate serves as the consensus mechanism for SERCA inhibition by other members of the SERCA regulatory subunit family including myoregulin and sarcolamban, and (ii) this consensus mechanism is utilized to regulate Ca^{2+} transport in skeletal and cardiac muscle, with important implications for therapeutic approaches to muscle dystrophy and heart failure.

© 2015 Published by Elsevier Inc.

[*]To whom correspondence should be addressed: espin049@umn.edu.

Publisher's Disclaimer: This is a PDF file of an unedited manuscript that has been accepted for publication. As a service to our customers we are providing this early version of the manuscript. The manuscript will undergo copyediting, typesetting, and review of the resulting proof before it is published in its final citable form. Please note that during the production process errors may be discovered which could affect the content, and all legal disclaimers that apply to the journal pertain.

Author Manuscript Author Manuscript Author Manuscript Author Manuscript

Keywords

sarcolipin; phospholamban; Ca^{2+} ATPase; SERCA; molecular dynamics simulations; heart failure; muscle dystrophy

1. Introduction

The muscle calcium pump (sarcoplasmic reticulum Ca^{2+}-ATPase, SERCA) is an integral membrane protein responsible for the transport of Ca^{2+} from the cytosol into the sarcoplasmic reticulum (SR) lumen of cardiac and skeletal muscle cells [1]. SERCA uses the energy derived from hydrolysis of one ATP molecule and the countertransported exchange of two protons [2,3]. Two membrane proteins are known to regulate SERCA activity: the 52-residue phospholamban (PLB) and the 31-residue sarcolipin (SLN). PLB is expressed in cardiac muscle and to a lesser extent in slow-twitch skeletal muscles, whereas SLN is predominantly expressed in skeletal muscles, but it is also expressed in atria [4,5]. Transient expression of SLN has also been found in the left ventricle in human Takotsubo cardiomyopathy [6].

SLN and PLB binding to SERCA have different functional outcomes. PLB controls Ca^{2+} affinity in a phosphorylation-dependent manner but has little or no effect on maximal velocity (V_{max}) [7], thus effectively regulating cardiac function during rest and exercise [8]. SLN also controls Ca^{2+} affinity of SERCA yet increases slippage of Ca^{2+} into the cytosol instead of the SR lumen [9], thus contributing to non-shivering thermogenesis in skeletal muscle [10]. Despite their distinct functional outcomes, SLN and PLB share important functional and structural features: (i) SLN and PLB both decrease the apparent Ca^{2+} affinity of SERCA [11]; (ii) they have high sequence identity, including homologous loss-of-function mutations: SLN mutants L8A and N11A and the analogous PLB mutants L31A and N34A, which all disrupt SERCA inhibition [12]; (iii) SLN and PLB bind to the same groove on the transmembrane domain of SERCA [13,14,15]; and (iv) the crystal structures of SERCA with bound PLB or SLN are virtually identical (RMSD=0.15-0.25 nm).

Super-physiological concentrations of Mg^{2+} have been used recently to obtain crystal structures of SLN-bound SERCA in an E1 conformation [13,14]. One crystal structure, obtained in the presence of 40 mM Mg^{2+}, shows a SLN-bound E1 structure with a single Mg^{2+} ion in the transport sites; this state was designated E1•Mg^{2+}-SLN [14]. It was proposed that SLN inhibits SERCA by stabilizing the E1•Mg^{2} state [14]. molecular dynamics (MD) simulation studies showed that E1•Mg^{2+} is not a functional intermediate of SERCA without bound subunit [16], and that Mg^{2+} ions do not bind to E1 under physiological conditions [16,17]. Based on this information, we hypothesize that SLN inhibits SERCA activity by populating a metal ion-free, protonated E1 state. To test this hypothesis, we performed protein pK_a calculations and microsecond-long MD simulations of SERCA-SLN starting from the crystal structure of E1•Mg^{2+}-SLN. By comparing our simulations of SERCA-SLN with our recent simulations of SERCA-PLB and subunit-free SERCA, we have identified a common intermediate for SERCA regulation in cardiac and skeletal muscle. We provide the first report that identifies a consensus mechanism for

Author Manuscript Author Manuscript Author Manuscript Author Manuscript

SERCA inhibition by SLN and PLB in atomic-level detail, with important implications for structure-based therapeutic approaches to heart failure and muscle dystrophy.

2. Materials and methods

2.1. Protein pK_a calculations

We used PROPKA 3.1 [18,19] to calculate the pK_a values of acidic residues in the transport sites of SERCA. PROPKA estimates empirical pK_a values of ionizable groups in proteins and protein-ligand complexes based on the 3D structure, and benefits from explicitly incorporating the Coulombic interactions that arise from mutually titrating residues via the Tanford-Roxby procedure [20].

2.2. Setting up SERCA-SLN for simulation

We used the crystal structure of E1•Mg^{2+}-SLN (PDB code: 3w5a [14]) as a starting structure for our simulations. We adjusted the charges on ionizable residues to correspond to their calculated values at pH ∼7.0, as follows. For E1•Mg^{2+}-SLN, residues E309, E771 and D800 were calculated to be ionized, and E908 was protonated. For Mg^{2+}-free SERCA-SLN, pK_a calculations predict residues E309 and D800 were ionized, and E771 and E908 were protonated. The complexes were inserted in a 12×12 nm bilayer of POPC and solvated using TIP3P water molecules. K^+, Mg^{2+}, and Cl^- ions were added to produce concentrations of 100 mM, 3 mM, and 110 mM, respectively. CHARMM36 force field topologies and parameters were used for the protein [21], lipid [22], water, K^+, and Cl^-. For Mg^{2+}, we used a set of new CHARMM parameters. [23].

2.3. Molecular dynamics simulations

MD simulations of SERCA-SLN were performed with NAMD 2.9 [24], periodic boundary conditions [25], particle mesh Ewald [26,27], a non-bonded cutoff of 0.9 nm, and a 2 fs time step. The NPT ensemble was maintained with a Langevin thermostat (310K) and an anisotropic Langevin piston barostat (1 atm). We performed two simulations: a 0.5-μs trajectory of E1•Mg^{2+}-SLN and a 2-μs trajectory of Mg^{2+}-unbound SERCA-SLN.

3. Results

3.1. Structural dynamics of E1•Mg^{2+}-SLN

We performed a 0.5-μs MD simulation of E1•Mg^{2+}-SLN to determine the structural dynamics of the crystallographic complex (Fig. 1A) in solution. We measured the backbone root-mean-square deviations (RMSD) for each functional domain of SERCA to determine the changes in SERCA (Fig. 1B). We found that the 10-helix transmembrane (TM) domain of SERCA rapidly settles to a plateau at 0.13 nm, indicating that its structure is nearly identical to that in the crystal structure of E1•Mg^{2+}-SLN. Each domain in the cytosolic headpiece of E1•Mg^{2+}-SLN undergoes relatively large-amplitude structural dynamics (RMSD=0.3-0.8 nm) in this time scale (Fig. 1B). The dynamic nature of the cytosolic headpiece, and in particular of the A domain, is in line with previous studies showing that the headpiece is inherently flexible in the E1 state in the absence and presence of PLB [16,17]. We also evaluated the structure and mobility of SLN in the complex. We found that

Author Manuscript Author Manuscript Author Manuscript Author Manuscript

residues R3-Q30 of SLN exclusively populate an α-helical structure in the trajectory. Root-mean square fluctuations (RMSF) of the main chain Cα atoms of SLN showed that, except for residues Ml, E2, and Y31, SLN has very low mobility in the complex (RMSF<0.15 nm, Fig. 1C).

3.2. Structure of transport site I in E1•Mg^{2+}-SLN

We measured intramolecular distances D800-E771 and E771-E908, and intermolecular distance $N11^{SLN}$-$G801^{SERCA}$ to determine the effects of SLN binding on the geometry of transport site I of E1•Mg^{2+}. Analysis of time evolution of interresidue distances showed a 0.5 nm decrease in the distance $N11^{SLN}$-$G801^{SERCA}$ (Fig. 2A), thus facilitating the formation of a hydrogen bond between the backbone oxygen of $G801^{SERCA}$ and the N_{δ} atom of $N11^{SLN}$ (Fig. 2B). The formation of this hydrogen bond occurs simultaneously with a 0.3-nm increase in the distance between E771 and D800, indicating that SLN pulls D800 away from site I even in the presence of bound Mg^{2+} (Fig. 2A,B). The distances D800-E771 and D800-E908 are ∼0.3 nm longer than those expected for competent transport site geometries [16] These results indicate that SLN disfavors the formation of a competent transport site I of SERCA.

3.3. Protein pK_a calculations of SERCA-SLN ± Mg^{2+}

We recently found that the distorted transport site geometry shown in Fig. 2B promotes protonation of residue E771 for PLB-bound SERCA [17]. Therefore, we used PROPKA to perform empirical pK_a calculations of acidic residues in the transport sites of E1•Mg^{2+}-SLN in the presence and absence of bound Mg^{2+}. The acidic residues analyzed here are E309, E771, D800, and E908. Predicted pK_a values of the crystal structure of Mg^{2+}-bound SERCA-SLN indicate that at resting pH of skeletal muscle (∼7.0 [28]), only residue E908 is protonated (Table 1). Identical protonation patterns were observed in p*K*a calculations performed on 6 independent 20-ns MD trajectories of Mg^{2+}-bound SERCA-SLN (Table 1); these trajectories were generated using the structure of E1•Mg^{2+}-SLN at t=0.5 μs as a starting point.

We performed six 20-ns MD trajectories of SERCA-SLN in the absence of bound Mg^{2+}, starting from the structure of E1•Mg^{2+}-SLN at t=0.5 μs. We found that upon Mg^{2+} removal, acidic residues E908 and E771 become protonated at physiological pH (Table 1). This protonation pattern is identical to that of SERCA-PLB reported recently by our group [17], indicating that PLB binding induces E771 protonation in the absence of bound Mg^{2+}. Therefore, we performed an additional MD simulation of SERCA-SLN protonated on E771 and E908 in the absence of bound Mg^{2+}. This simulation was performed to evaluate the structural properties of the protonated complex, and to determine whether E1•Mg^{2+}-SLN is populated at physiologically relevant Mg^{2+} concentrations.

3.4. Structural dynamics of E1•H^{+}_{771}-SLN

We performed a 2-μs MD simulation of the SERCA-SLN complex starting from the structure of E1•Mg^{2+}-SLN at t=0.5 μs, but in the absence of bound Mg^{2+}. Time evolution of RMSD values for each functional domain of SERCA showed that the TM domain undergoes minor structural changes (RMSD<0.2 nm), but it is structurally stable in the trajectory

Author Manuscript Author Manuscript Author Manuscript Author Manuscript

(Supplementary Figure S1). As in E1•Mg^{2+}-SLN, the cytosolic domain is mobile; however, all three N, A and P domains become less mobile after *t*=1.3 μs (Supplementary Figure S1). Calculation of RMSF values for SLN showed that, except for residues M1, E2 and Y31, SLN has very low mobility in the complex (RMSF<0.15 nm) and that it populates a stable α-helical structure in the trajectory. The RMSF pattern is nearly identical to that of E1•Mg^{2+}-SLN, indicating that Mg^{2+} binding does not play a role on the structural dynamics of SLN.

Analysis of the Mg^{2+}-SERCA interactions in or near the transport sites showed that Mg^{2+} binds, albeit transiently (t<4 ns), near residues E58, D59, and E109 (Supplementary Figure S2). These residues are located near the entrance to the transport sites, but Mg^{2+} binding to these sites occur only three times in the trajectory, and Mg^{2+} does not enter the transport sites in the trajectory. This data and our p*K*a calculations indicate that at physiological conditions, SLN binding to SERCA does not stabilize a E1•Mg^{2+} state, but instead an E1 state protonated on E771 and E908. We designate this state E1•H^{+}_{771}-SLN.

3.5. Structural comparison of transport site I in E1•H^{+}_{771}-SLN and E1•H^{+}_{771}-PLB

We measured the distances D800-E771 and E771-E908 to evaluate the structural arrangement of transport site I in E1•H^{+}_{771}-SLN (Fig. 3A). Analysis of the time-dependent distance plots show that interresidue distances in transport site I do not fluctuate substantially in the trajectory. Comparison between the interresidue distances in E1•H^{+}_{771}-SLN with distance distributions calculated from three independent MD trajectories of E1•H^{+}_{771}-PLB (Fig. 3B) indicate that both SLN and PLB produce identical structural arrangements of transport site I of the E1 state (Fig. 3C).

We recently showed that the transport sites of PLB-bound SERCA bind K^+ ions transiently and non-specifically [17]. Therefore, we investigated the K^+ interactions with the transport sites of E1•H^{+}_{771}-SLN and compared them with those of E1•H^{+}_{771}-PLB. We found that transport sites of E1•H^{+}_{771}-SLN are occupied by K^+ at least 80% of the time, but the residence time of K^+ is ≤5 ns. K^+ binds only transiently to the transport sites of E1•H^{+}_{771}-SLN, an identical behavior observed in the inhibited transport sites of E1•H^{+}_{771}-PLB [17]. We found that K^+ ions bind non-specifically to nine identical positions we have previously identified in PLB-bound E1•H^{+}_{771} (Fig. 4A). The binding preference for each site is different for SLN- and PLB-bound SERCA (Fig. 4B). Despite this variability, we found that K^+ sites 1 and 2 are occupied for ∼40% of the time in both SLN- and PLB-bound E1•H^{+}_{771}. These sites are located near residue D800, which is ionized in E1•H^{+}_{771}. Therefore, neutralization of D800 by K^+ is a conserved feature in both E1•H^{+}_{771}-SLN and E1•H^{+}_{771}-PLB. These results indicate that PLB and SLN binding to SERCA populate identical structurally stable but incompetent transport site I. Thus, SLN and PLB inhibit SERCA similarly by populating E1•H^{+}_{771},

4. Discussion

Protein pK_a calculations and MD simulations showed that SLN induces structural changes in the transport sites that correspond to those previously identified as inhibitory. This local structural change occurs in the presence and absence of bound Mg^{2+}, indicating that the

Author Manuscript Author Manuscript Author Manuscript Author Manuscript

effect of SLN on SERCA is independent of the type of metal ion bound in the transport sites.

Protein p*K*a calculations and MD simulations showed that E1•Mg^{2+} is not the main intermediate stabilized by SLN. Instead, SLN binding to SERCA alters the geometry of transport site I and populates a protonated E1 intermediate, E1•H^{+}_{771}. Comparison between our data and previous MD simulations of SERCA-PLB revealed that both SLN and PLB inhibit the SERCA by populating an identical intermediate, E1•H^{+}_{771}. We recently showed that PLB-bound E1•H^{+}_{771} serves as a kinetic trap that depresses but does not abolish SERCA activity at normal physiological conditions [17]. These findings are in line with experimental data showing that both SLN and PLB decrease the apparent Ca^{2+} affinity of SERCA [11,12].

It is possible that other newly-discovered SERCA regulators sarcolamban (SCL) [29] and myoregulin (MLN) [30] control Ca^{2+} affinity by populating E1•H^{+}_{771} because they share structural and functional similarity with PLB and SLN. Therefore, we propose that this mechanism for inhibition of Ca^{2+} transport applies to both cardiac and skeletal muscle. These findings have profound therapeutic implications because Ca^{2+} dysregulation is a hallmark of muscle and cardiovascular diseases. For example, disruption of the SERCA-PLB complex in cardiac muscle can be used to normalize Ca^{2+} cycling in diseased cardiomyocytes, thus improving cardiac function in heart failure [31,32,33,34]. In skeletal muscle, over-expression of SERCA enhances SR Ca^{2+}-uptake, excitation-contraction coupling, and Ca^{2+} clearance from sarcoplasm, thus mitigating Duchenne muscular dystrophy [35]. Identification of E1•H^{+}_{771} as the inhibitory mechanism opens new doors for structure-based strategies to stimulate SERCA and Ca^{2+} transport in muscle and heart disease. This includes the discovery of small molecule activators of SERCA and gene therapy strategies to neutralize subunit inhibition.

Further studies will be needed to answer questions regarding the functional differences among these regulatory proteins. For example, if PLB and SLN induce the same structural changes in the transport sites (Fig. 3) and populate the same inhibitory intermediate, why is only SLN able to uncouple SERCA [36]? What are the mechanisms by which the luminal tail in SLN regulates SERCA [11]? What about other post-translational protein modifications such as SLN acylation [37]? What is the role of SLN self-oligomerization in SERCA regulation [38]? Complementary experiments and simulation studies on SERCA regulation will be needed to test these questions directly.

5. Conclusion

We have used protein pK_a calculations and microsecond MD simulations to demonstrate that SLN-bound SERCA is protonated at residue E771 and does not bind Mg^{2+}. These findings indicate that SLN binding to SERCA does not populate E1•Mg^{2+} but an E1 intermediate protonated on E771, E1•H^{+}_{771}. Comparison with our previous MD simulations of SERCA-PLB showed remarkable similarities in the effects of SLN and PLB binding to SERCA, including (i) control of transport site geometry, (ii) formation of E1•H^{+}_{771}, and (iii) transient binding of K^{+} but not Mg^{2+} in the transport sites. We propose that both SLN and PLB

Author Manuscript Author Manuscript Author Manuscript Author Manuscript

inhibit SERCA activity by populating an identical inhibited E1 state of the pump. This partially-protonated intermediate serves as the consensus mechanism for SERCA inhibition by other members of the SERCA regulatory subunit family. We conclude that this consensus mechanism is utilized to regulate Ca^{2+} transport in skeletal and cardiac muscle, with important implications for therapeutic approaches to muscular dystrophy and heart failure.

Supplementary Material

Refer to Web version on PubMed Central for supplementary material.

Acknowledgments

This work was supported by grants to L.M.E-F. from the American Heart Association (12SDG12060656) and to D.D.T. from the NIH (R01GM27906). This project made extensive use of the outstanding high-performance computing resources at the Minnesota Supercomputing Institute.

References

1. Palmgren MG, Nissen P. P-type ATPases. Annu Rev Biophys. 2011; 40:243–266. [PubMed: 21351879]
2. Yu X, Carroll S, Rigaud JL, Inesi G. H+ countertransport and electrogenicity of the sarcoplasmic reticulum Ca2+ pump in reconstituted proteoliposomes. Biophys J. 1993; 64:1232–1242. [PubMed: 8388268]
3. Zafar S, Hussain A, Liu Y, Lewis D, Inesi G. Specificity of ligand binding to transport sites: Ca2+ binding to the Ca2+ transport ATPase and its dependence on H+ and Mg2+ Arch Biochem Biophys. 2008; 476:87–94. [PubMed: 18485884]
4. Babu GJ, Bhupathy P, Carnes CA, Billman GE, Periasamy M. Differential expression of sarcolipin protein during muscle development and cardiac pathophysiology. J Mol Cell Cardiol. 2007; 43:215–222. [PubMed: 17561107]
5. Vangheluwe P, Schuermans M, Zador E, Waelkens E, Raeymaekers L, Wuytack F. Sarcolipin and phospholamban mRNA and protein expression in cardiac and skeletal muscle of different species. Biochem J. 2005; 389:151–159. [PubMed: 15801907]
6. Nef HM, Mollmann H, Troidl C, Kostin S, Voss S, Hilpert P, Behrens CB, Rolf A, Rixe J, Weber M, Hamm CW, Elsasser A. Abnormalities in intracellular Ca2+ regulation contribute to the pathomechanism of Tako-Tsubo cardiomyopathy. European Heart Journal. 2009; 30:2155–2164. [PubMed: 19525500]
7. MacLennan DH, Kranias EG. Phospholamban: a crucial regulator of cardiac contractility. Nat Rev Mol Cell Biol. 2003; 4:566–577. [PubMed: 12838339]
8. Gielen S, Schuler G, Adams V. Cardiovascular effects of exercise training: molecular mechanisms. Circulation. 2010; 122:1221–1238. [PubMed: 20855669]
9. Mall S, Broadbridge R, Harrison SL, Gore MG, Lee AG, East JM. The presence of sarcolipin results in increased heat production by Ca(2+)-ATPase. J Biol Chem. 2006; 281:36597–36602. [PubMed: 17018526]
10. Bal NC, Maurya SK, Sopariwala DH, Sahoo SK, Gupta SC, Shaikh SA, Pant M, Rowland LA, Bombardier E, Goonasekera SA, Tupling AR, Molkentin JD, Periasamy M. Sarcolipin is a newly identified regulator of muscle-based thermogenesis in mammals. Nat Med. 2012; 18:1575–1579. [PubMed: 22961106]
11. Gorski PA, Glaves JP, Vangheluwe P, Young HS. Sarco(endo)plasmic reticulum calcium ATPase (SERCA) inhibition by sarcolipin is encoded in its luminal tail. J Biol Chem. 2013; 288:8456–8467. [PubMed: 23362265]
12. Odermatt A, Becker S, Khanna VK, Kurzydlowski K, Leisner E, Pette D, MacLennan DH. Sarcolipin regulates the activity of SERCA1, the fast-twitch skeletal muscle sarcoplasmic reticulum Ca2+-ATPase. J Biol Chem. 1998; 273:12360–12369. [PubMed: 9575189]

Author Manuscript Author Manuscript Author Manuscript Author Manuscript

13. Winther AM, Bublitz M, Karlsen JL, Moller JV, Hansen JB, Nissen P, Buch-Pedersen MJ. The sarcolipin-bound calcium pump stabilizes calcium sites exposed to the cytoplasm. Nature. 2013; 495:265–269. [PubMed: 23455424]
14. Toyoshima C, Iwasawa S, Ogawa H, Hirata A, Tsueda J, Inesi G. Crystal structures of the calcium pump and sarcolipin in the Mg2+-bound E1 state. Nature. 2013; 495:260–264. [PubMed: 23455422]
15. Akin BL, Hurley TD, Chen Z, Jones LR. The structural basis for phospholamban inhibition of the calcium pump in sarcoplasmic reticulum. J Biol Chem. 2013; 288:30181–30191. [PubMed: 23996003]
16. Espinoza-Fonseca LM, Autry JM, Thomas DD. Microsecond molecular dynamics simulations of Mg(2)(+)-and K(+)-bound E1 intermediate states of the calcium pump. PLoS One. 2014; 9:e95979. [PubMed: 24760008]
17. Espinoza-Fonseca LM, Autry JM, Ramirez-Salinas GL, Thomas DD. Atomic-level mechanisms for phospholamban regulation of the calcium pump. Biophys J. 2015; 107:1697–1708. [PubMed: 25863061]
18. Olsson MHM, Sondergaard CR, Rostkowski M, Jensen JH. PROPKA3: Consistent Treatment of Internal and Surface Residues in Empirical pK(a) Predictions. Journal of Chemical Theory and Computation. 2011; 7:525–537.
19. Sondergaard CR, Olsson MHM, Rostkowski M, Jensen JH. Improved Treatment of Ligands and Coupling Effects in Empirical Calculation and Rationalization of pK(a) Values. Journal of Chemical Theory and Computation. 2011; 7:2284–2295.
20. Tanford C, Roxby R. Interpretation of protein titration curves. Application to lysozyme. Biochemistry. 1972; 11:2192–2198. [PubMed: 5027621]
21. Best RB, Zhu X, Shim J, Lopes PE, Mittal J, Feig M, Mackerell AD Jr. Optimization of the additive CHARMM all-atom protein force field targeting improved sampling of the backbone phi, psi and side-chain chi(1) and chi(2) dihedral angles. J Chem Theory Comput. 2012; 8:3257–3273. [PubMed: 23341755]
22. Klauda JB, Venable RM, Freites JA, O'Connor JW, Tobias DJ, Mondragon-Ramirez C, Vorobyov I, MacKerell AD Jr, Pastor RW. Update of the CHARMM all-atom additive force field for lipids: validation on six lipid types. J Phys Chem B. 2010; 114:7830–7843. [PubMed: 20496934]
23. Allner O, Nilsson L, Villa A. Magnesium Ion-Water Coordination and Exchange in Biomolecular Simulations. Journal of Chemical Theory and Computation. 2012; 8:1493–1502.
24. Phillips JC, Braun R, Wang W, Gumbart J, Tajkhorshid E, Villa E, Chipot C, Skeel RD, Kale L, Schulten K. Scalable molecular dynamics with NAMD. J Comput Chem. 2005; 26:1781–1802. [PubMed: 16222654]
25. Weber W, Hünenberger PH, McCammon JA. Molecular Dynamics Simulations of a Polyalanine Octapeptide under Ewald Boundary Conditions: Influence of Artificial Periodicity on Peptide Conformation. J Phys Chem B. 2000; 104:3668–3675.
26. Darden T, York D, Pedersen L. Particle mesh Ewald: An N•log(N) method for Ewald sums in large systems. J Chem Phys. 1993; 98:10089–10092.
27. Essmann U, Perera L, Berkowitz ML. A smooth particle mesh Ewald method. J Chem Phys. 1995; 103:8577–8593.
28. Pan JW, Hamm JR, Rothman DL, Shulman RG. Intracellular pH in human skeletal muscle by 1H NMR. Proc Natl Acad Sci U S A. 1988; 85:7836–7839. [PubMed: 3186694]
29. Magny EG, Pueyo JI, Pearl FMG, Cespedes MA, Niven JE, Bishop SA, Couso JP. Conserved Regulation of Cardiac Calcium Uptake by Peptides Encoded in Small Open Reading Frames. Science. 2013; 341:1116–1120. [PubMed: 23970561]
30. Anderson DM, Anderson KM, Chang CL, Makarewich CA, Nelson BR, McAnally JR, Kasaragod P, Shelton JM, Liou J, Bassel-Duby R, Olson EN. A micropeptide encoded by a putative long noncoding RNA regulates muscle performance. Cell. 2015; 160:595–606. [PubMed: 25640239]
31. Iwanaga Y, Hoshijima M, Gu Y, Iwatate M, Dieterle T, Ikeda Y, Date MO, Chrast J, Matsuzaki M, Peterson KL, Chien KR, Ross J Jr. Chronic phospholamban inhibition prevents progressive cardiac dysfunction and pathological remodeling after infarction in rats. J Clin Invest. 2004; 113:727–736. [PubMed: 14991071]

Author Manuscript Author Manuscript Author Manuscript Author Manuscript

32. Marks AR. Calcium cycling proteins and heart failure: mechanisms and therapeutics. J Clin Invest. 2013; 123:46–52. [PubMed: 23281409]

33. del Monte F, Harding SE, Dec GW, Gwathmey JK, Hajjar RJ. Targeting phospholamban by gene transfer in human heart failure. Circulation. 2002; 105:904–907. [PubMed: 11864915]

34. Greenberg B, Yaroshinsky A, Zsebo KM, Butler J, Felker GM, Voors AA, Rudy JJ, Wagner K, Hajjar RJ. Design of a phase 2b trial of intracoronary administration of AAV1/SERCA2a in patients with advanced heart failure: the CUPID 2 trial (calcium up-regulation by percutaneous administration of gene therapy in cardiac disease phase 2b). JACC Heart Fail. 2014; 2:84–92. [PubMed: 24622121]

35. Goonasekera SA, Lam CK, Millay DP, Sargent MA, Hajjar RJ, Kranias EG, Molkentin JD. Mitigation of muscular dystrophy in mice by SERCA overexpression in skeletal muscle. J Clin Invest. 2011; 121:1044–1052. [PubMed: 21285509]

36. Sahoo SK, Shaikh SA, Sopariwala DH, Bal NC, Periasamy M. Sarcolipin protein interaction with sarco(endo)plasmic reticulum Ca2+ ATPase (SERCA) is distinct from phospholamban protein, and only sarcolipin can promote uncoupling of the SERCA pump. J Biol Chem. 2013; 288:6881–6889. [PubMed: 23341466]

37. Montigny C, Decottignies P, Le Marechal P, Capy P, Bublitz M, Olesen C, Moller JV, Nissen P, le Maire M. S-palmitoylation and s-oleoylation of rabbit and pig sarcolipin. J Biol Chem. 2014; 289:33850–33861. [PubMed: 25301946]

38. Autry JM, Rubin JE, Pietrini SD, Winters DL, Robia SL, Thomas DD. Oligomeric interactions of sarcolipin and the Ca-ATPase. J Biol Chem. 2011; 286:31697–31706. [PubMed: 21737843]

Author Manuscript Author Manuscript Author Manuscript Author Manuscript

Highlights

- SERCA-SLN does not populate the E1•Mg^{2+} intermediate in solution.
- SLN binding populates an inhibited SERCA intermediate protonated at E771, E1•H^{+}_{771}.
- SLN and PLB inhibit SERCA by an identical protonated E1 intermediate E1•H^{+}771.
- The family of SERCA regulatory proteins shares a consensus inhibitory mechanism.

Author Manuscript Author Manuscript Author Manuscript Author Manuscript

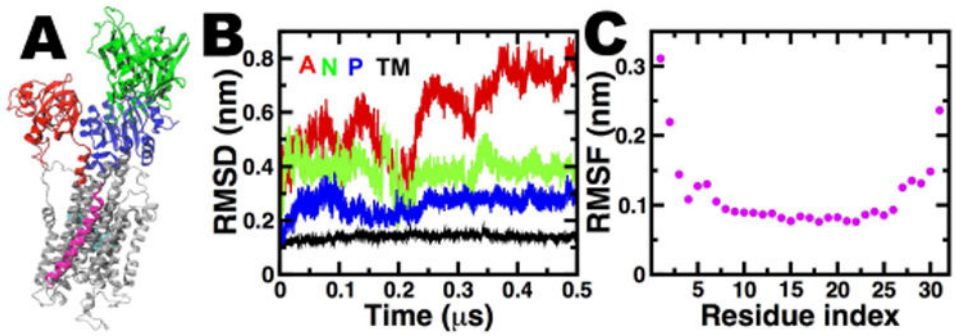

Fig. 1. Structural dynamics of E1•Mg^{+}-SLN

(A) Crystal structure of the E1•Mg^{+}-SLN. SERCA is colored according to its four functional domains: N (green), P (blue), A (red), and TM (grey); SLN is shown in magenta. (B) Time-dependent changes in RMSD of SERCA domains. RMSD of the TM domain was calculated using backbone alignment for TM helices of the pump; RMSD of A, N, and P domains was calculated by aligning the backbone of the cytosolic headpiece. (C) C_{α} RMSF of SLN calculated from the MD trajectory.

Author Manuscript Author Manuscript Author Manuscript Author Manuscript

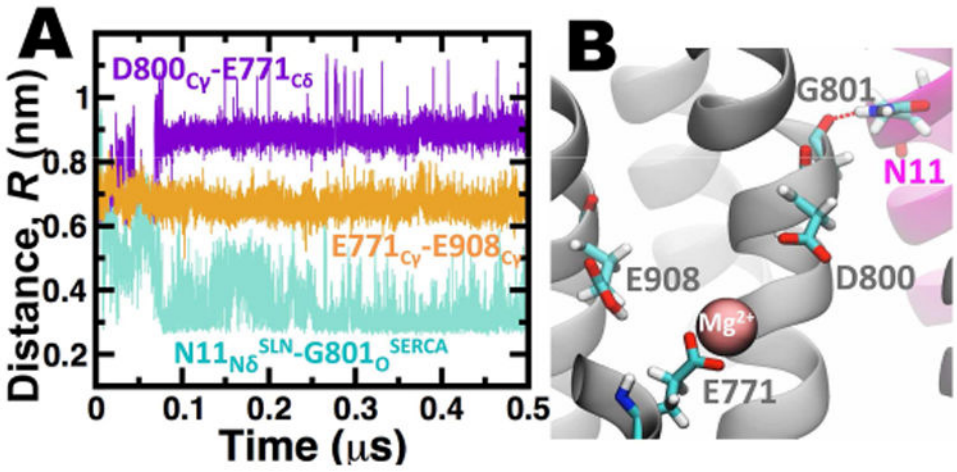

Fig. 2. Structure of transport site I in E1•Mg^{2+}-SLN

(A) Distance evolution between residues D800-E771 and E771-E908 of SERCA, and G801 of SERCA and N11 of SLN. C_γ-C_δ, and C_δ-C_δ distances were calculated for D800-E771 and E771-E908, respectively. The distance $N11^{SLN}$-$G801^{SERCA}$ was calculated between the backbone oxygen of G801 and the N_δ of N11. (B) Structure of transport site I at the end of the 0.5-μs MD simulation. SERCA and SLN are shown as grey and magenta ribbons, residues in the transport sites as sticks, and Mg^{2+} as a sphere.

Author Manuscript Author Manuscript Author Manuscript Author Manuscript

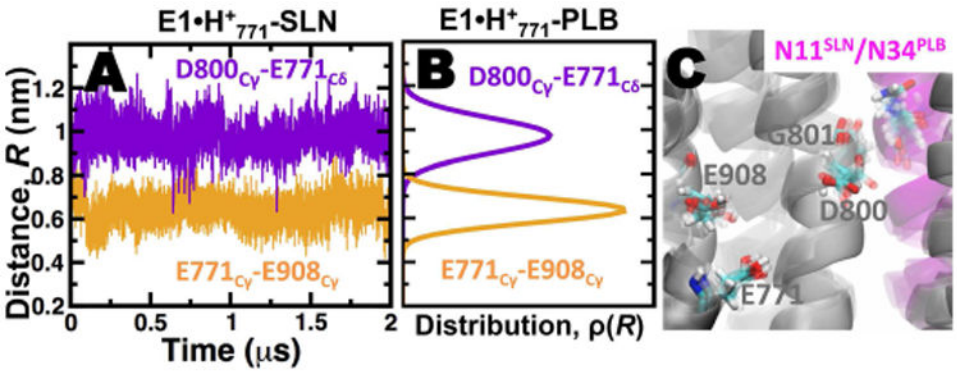

Fig. 3. Geometric comparison of transport site I of E1•H$^+_{771}$-SLN and E1•H$^+_{771}$-PLB

(A) Distances were calculated between C_δ-C_δ and C_δ-C_γ atoms for E771-E908 and D800-E771, respectively. (B) For comparison, we plotted distance distributions for residue pairs D800-E771 and E771-908 of E1•H$^+_{771}$-PLB. Distributions were obtained by combining three 1-μs trajectories of E1•H$^+_{771}$-PLB reported in reference [17]. (C) Superposition of E1•H$^+_{771}$-SLN at *t=2* μs onto three structures of E1•H$^+_{771}$-PLB at the end three independent 1-μs MD simulations. We show that SLN and PLB produce an identical structural arrangement of transport site I.

Author Manuscript Author Manuscript Author Manuscript Author Manuscript

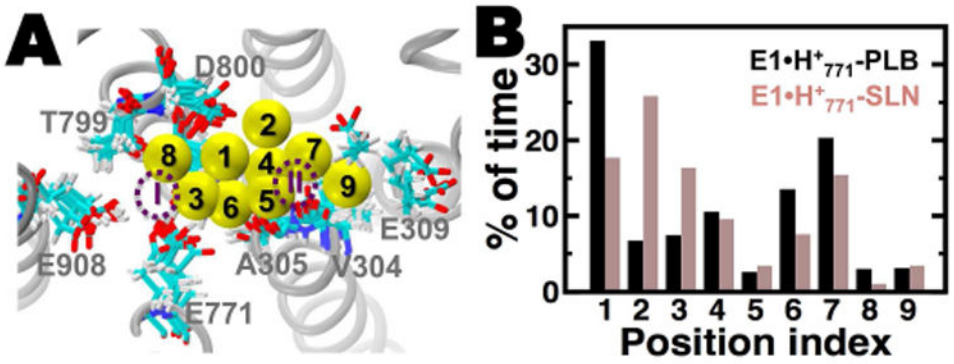

Fig. 4. Transient K^+ ion interactions in the transport sites of E1•H^+-SLN and E1•H^+-PLB

(A) Location of the nine different positions occupied by K^+ (yellow spheres) in the transport sites of E1•H^+. Each position is labeled from 1 to 9. The dashed circles show the approximate location of transport sites I and II. TM helices are represented by grey ribbons and cation-binding residues are shown as sticks. (B) Percent of time K^+ spends at each position. The values for E1•H^+-PLB represent the average from three independent 1-μs simulations reported in [17].

Author Manuscript

Author Manuscript

Author Manuscript

Author Manuscript

Table 1

Predicted pK_a values of acidic residues in the transport sites

State	E309	E771	D800	E908
SERCA-SLN, +Mg^{2+} (x-ray)[1,3]	5.6	6.6	3.0	8.8
SERCA-SLN, +Mg^{2+} (MD)[2,3]	6.1±0.1	4.8±0.2	4.8±0.1	7.5±0.1
SERCA-SLN, -Mg^{2+} (MD)[2,3]	5.3±0.1	8.9±0.1	5.7±0.3	7.7±0.1
SERCA-PLB (MD)[2,4]	5.4±0.3	9.2±0.2	6.1±0.1	7.9±0.2

[1] Reported values are mean± SE.

[2] pK_a values calculated using a single crystal structure (PDB code: 3w5a).

[3] +Mg^{2+} and −Mg^{2+} indicate the presence and absence of a single Mg^{2+} ion bound in the transport sites.

[4] pK_a values from reference [17]